A MICHELSON-TYPE RADIO INTERFEROMETER FOR UNIVERSITY EDUCATION

Jin Koda[1], James Barrett[1], Tetsuo Hasegawa[2,3], Masahiko Hayashi[3], Gene Shafto[1], Jeff Slechta[1], and
Stanimir Metchev[1,4]

Accepted for publication in American Journal of Physics, January 14, 2016

ABSTRACT

We report development of a simple and affordable radio interferometer suitable as an educational laboratory experiment. The design of this interferometer is based on the Michelson & Pease stellar optical interferometer, but operates at a radio wavelength ($\sim$11 GHz; $\sim$ 2.7 cm); thus the requirement for optical accuracy is much less stringent. We utilize a commercial broadcast satellite dish and feedhorn. Two flat side mirrors slide on a ladder, providing baseline coverage. This interferometer resolves and measures the diameter of the Sun, a nice daytime experiment which can be carried out even in marginal weather (i.e., partial cloud cover). Commercial broadcast satellites provide convenient point sources for comparison to the Sun's extended disk. We describe the mathematical background of the adding interferometer, the design and development of the telescope and receiver system, and measurements of the Sun. We present results from a students' laboratory report. With the increasing importance of interferometry in astronomy, the lack of educational interferometers is an obstacle to training the future generation of astronomers. This interferometer provides the hands-on experience needed to fully understand the basic concepts of interferometry.

1. INTRODUCTION

The future of radio astronomy relies strongly on interferometers (e.g., ALMA, EVLA, VLTI, aperture masking techniques). From our experience at interferometer summer schools at the Nobeyama Radio Observatory and at the CARMA Observatory, we are convinced that hands-on experiments are critical to a full understanding of the concepts of interferometry. It is difficult, if not impossible, to obtain guaranteed access to professional interferometers for university courses. Therefore, we built a low-cost radio interferometer for the purpose of education and developed corresponding syllabi for undergraduate and graduate astronomy lab courses.

This experiment teaches the basic concept of interferometry using the technique developed by Michelson & Peace in the early 20th century (Michelson & Pease 1921). They measured the diameter of Betelgeuse, one of the brightest stars in the sky, with a simple optical interferometer. Such optical interferometry needs high precision telescope optics. The same experiment becomes much easier when measuring the diameter of the Sun at radio wavelength; the acceptable errors in the optics scale with the wavelength.

Figure 1 shows a conceptual sketch of the Michelson radio interferometer for education. This type of interferometer, adding signals instead of multiplying them, is called an adding interferometer. We discuss the mathematical background of the adding interferometer in §2, design and development of the telescope and receiver system in

§3, telescope setup and measurements in §4, and results from a students' lab report in §5. What we present here is only one realization of the concept. Creative readers could modify any part to meet the educational needs and constraints at their own institutions. For example, the astronomical measurement, the construction and tests of of telescope, receiver system, and other components can be separate lab projects.

The best known Michelson interferometer is the one used for the Michelson-Morley experiment (Michelson & Morley 1887). It is one of the most important classical experiments taught in both lecture and laboratory courses (Wolfson & Pasachoff 1999; Melissinos & Napolitano 2003; Serway & Jewett 2013; Bennett et al. 2013). Many studies and applications have appeared in this journal(Fang et al. 2013; Rudmin et al. 1980; Matthys & Pedrotti 1982; da Costa, Kiedansky & Siri 1988; Diamond et al. 1990; Mellen 1990; Norman 1992; Belansky, Richard & Wanser 1993; Kiess & Berg 1996; Nachman, Pellegrino & Bernstein 1997; Fox et al. 1999), and recently the Michelson interferometer is being applied to the detection of gravitational waves (Kuroda et al. 1999; Abbott et al. 2009; Harry & LIGO Scientific Collaboration 2010). The Michelson stellar interferometer is an application of the same physical concept of interference, in this case, to a light source in the sky.

The theoretical basis of the Michelson stellar interferometer was already established in the Michelson and Peace's original work (Michelson & Pease 1921) and has been used in radio interferometry, especially in its early history (Pawsey & Bracewell 1955; Steinberg & Lequeux 1963; Christiansen & Högbom 1985; Wilson, Rohlfs & Hüttemeister 2013). This adding interferometer is the type used in modern astronomy at optical and near-infrared wavelengths (Shao & Colavita 1992; Quirrenbach 2001) though modern radio interferometers are of a different type, multiplying signals instead of adding them (Taylor Carilli; Thompson, Moran & Swenson 2007). For educational purposes, some studies in this journal showed

jin.koda@stonybrook.edu

[1] Department of Physics and Astronomy, Stony Brook University, Stony Brook, NY 11794-3800
[2] National Astronomical Observatory of Japan, NAOJ Chile Observatory, Joaquín Montero 3000 Oficina 702, Vitacura, Santiago 763-0409, Chile
[3] National Astronomical Observatory of Japan, 2-21-1 Osawa, Mitaka, Tokyo 181-0015, Japan
[4] Department of Physics and Astronomy, The University of Western Ontario, 1151 Richmond St, London, ON N6A 3K7, Canada

that the concept of the stellar interferometer could be demonstrated in an indoor laboratory setup using an artificial light source (Pryor 1959; Illarramendi et al. 2014). In professional optical astronomy, the technique is now being applied for advanced research (Shao & Colavita 1992; Quirrenbach 2001; Monnier 2003).

2. MATHEMATICAL BACKGROUND

The mathematical basis of the stellar interferometer was presented in Michelson and Peace's original work(Michelson & Pease 1921) and can be found in textbooks (Pawsey & Bracewell 1955; Steinberg & Lequeux 1963; Christiansen & Högbom 1985; Wilson, Rohlfs & Hüttemeister 2013). Here we describe the basic equations at a mathematical level that college students can follow.

We start from the geometric delay calculation (§2.1) and explain the total power, the parameter that we measure, in §2.2. We will show an example of how a point source (i.e., a commercial broadcast satellite) appears in §2.3. We will then discuss the case of an extended source. We prove that an interferometer measures Fourier components and define visibility in §2.4. We will explain how visibility is measured with our interferometer, and how the Sun's diameter is derived in §2.5.

2.1. Geometric Delay

Interferometers mix signals received at two different positions (position 1 & 2 in Figure 2). In our radio interferometer, the signals that arrive at the two side mirrors (Figure 1) are guided to the antenna and mixed. The separation between the two mirrors, called baseline length B, causes a time delay τ in the arrival of the signal at position 2 because of the geometry (Figure 2). Using the angles of the telescope pointing θ and to an object in the sky θ_0, a simple geometric calculation provides the delay,

$$\tau = \frac{B\sin(\theta - \theta_0)}{c} \sim \frac{B(\theta - \theta_0)}{c} \qquad (1)$$

where c is the speed of light. We used the small angle approximation, $\sin(\theta - \theta_0) \sim \theta - \theta_0$, since most astronomical objects have a small angular size.

2.2. Total Power

Radio signals are electromagnetic radiation and can be described in terms of an electric field E and a magnetic field B. For simplicity, we consider only the electric field E in the following calculations (but this simplification does not lose the generality of the discussion). If we define the radio signal at frequency ν that is detected at position 1 (or reflected if a mirror is there) at time t as,

$$E_1(t) = E(\theta_0)\cos[2\pi\nu t], \qquad (2)$$

the signal that is detected at position 2 at the same time is,

$$E_2(t) = E(\theta_0)\cos[2\pi\nu(t - \tau)], \qquad (3)$$

because of the geometric delay τ.

An adding interferometer adds the two signals and measures total power of the two. The total electric field is

$$E_{\text{tot}}(t) = E_1(t) + E_2(t). \qquad (4)$$

The radio frequency ν is typically large compared to a data sampling rate. Hence, the total power $P(\theta)$, detected by a receiver, is a time average (or integration). Using the notation $< ... >$ for the time average, we obtain

$$P(\theta) = \left\langle E_{\text{tot}}^2(\theta) \right\rangle \qquad (5)$$

$$= \left\langle E^2(\theta_0)\left(\cos[2\pi\nu t] + \cos[2\pi\nu(t - \tau)]\right)^2 \right\rangle \qquad (6)$$

$$= \left\langle E^2(\theta_0)\left(\cos^2[2\pi\nu t] + \cos^2[2\pi\nu(t - \tau)]\right.\right.$$
$$\left.\left. +2\cos[2\pi\nu t]\cos[2\pi\nu(t - \tau)]\right)\right\rangle \qquad (7)$$

$$= E^2(\theta_0)[1 + \cos(2\pi\nu\tau)] \qquad (8)$$

In going from eq (7) to (8) we used the transformations: $\cos^2 A = (\cos 2A + 1)/2$ for the first and third terms and $2\cos A\cos B = \cos(A + B) + \cos(A - B)$ for the second term. In addition, because of the high frequency, ν, all terms with $\langle\cos(*\nu t)\rangle$, $\langle\sin(*\nu t)\rangle$, etc, vanish when time averaged, and only the terms with no t dependence remain. Using equation (1) with the small angle approximation, this becomes

$$P(\theta) = E^2(\theta_0)[1 + \cos(2\pi B_\lambda(\theta - \theta_0))] \qquad (9)$$

where $B_\lambda \equiv B/\lambda$ is a normalized baseline length and λ is the wavelength ($\lambda = c/\nu$).

Equation (9) can be generalized for an extended object as

$$P(\theta) = \int \mathcal{E}(\theta_0)d\theta_0[1 + \cos(2\pi B_\lambda(\theta - \theta_0))], \qquad (10)$$

where $\mathcal{E}(\theta_0)$ is an intensity/energy density distribution of the object. Our adding interferometer measures $P(\theta)$; we slew the telescope across the object in the azimuthal direction and obtain *fringes*, i.e., variations in the power as a function of θ.

2.3. Point Source

The energy density of a point source is a δ-function at the position of the object $\theta_0 = \theta_c$. By adopting the coordinate origin to make $\theta_c = 0$, it is

$$\mathcal{E}(\theta_0) = \mathcal{E}_0\delta(\theta_0). \qquad (11)$$

Combining with eq. (10), we obtain

$$P(\theta) = \mathcal{E}_0[1 + \cos(2\pi B_\lambda(\theta - \theta_0))]. \qquad (12)$$

As we sweep the telescope from one side of the object to the other, we should see a sinusoidal power response as a function of θ.

Figure 3 (*top*) shows the theoretical fringe pattern from a point source. Our satellite dish (and any other radio telescope) has a directivity; its response pattern tapers off away from the center. The pattern that we actually obtain is attenuated by the dish response pattern (beam pattern) as shown in Figure 3 (*bottom*). Commercial broadcast satellites are very small in angle and approximate point sources.

Fringe measurements are useful in determining the baseline length B_λ. The total power is zero when the normalized baseline is $B_\lambda(\theta - \theta_0) = n + 1/2$, where n is an integer. The separation between adjacent null positions is $\delta\theta = 1/B_\lambda = \lambda/B$.
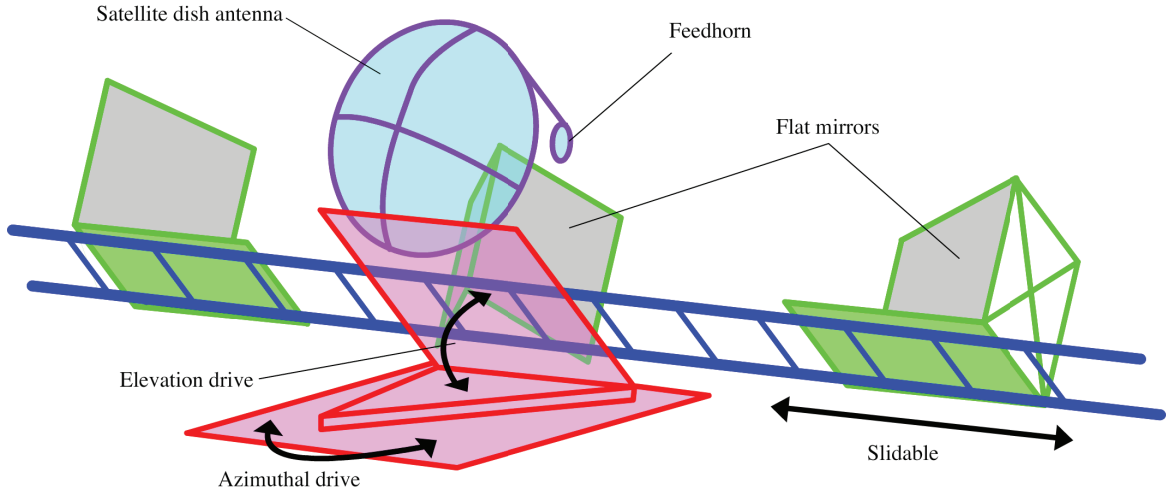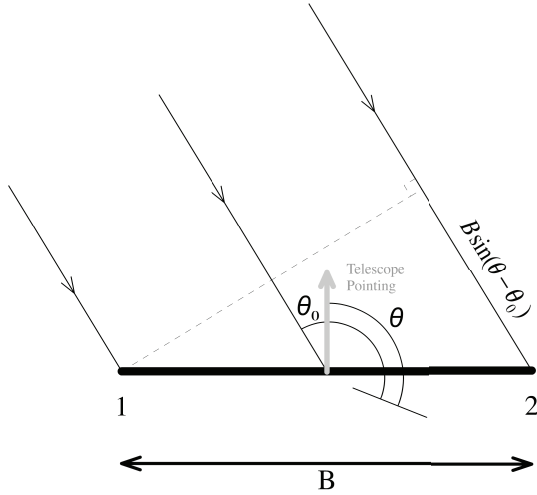
FIG. 1.— Conceptual sketch of the Michelson radio interferometer.

$$E_1(\theta) = E(\theta_0)\cos[2\pi\nu t] \qquad E_2(\theta) = E(\theta_0)\cos[2\pi\nu(t-\tau)]$$

FIG. 2.— Schematic illustration of signal detection with two detectors separated by the baseline length B. The direction of the telescope pointing is θ and that to an object in sky is θ_0, both from an arbitrary origin.

2.4. Extended Source and Visibility

An astronomical object is often extended. In general, an interferometer measures the Fourier transform of the energy density distribution $\mathcal{E}(\theta_0)$. Here we prove this.

From eq. (10) we define the visibility $V_0(B_\lambda)$ as follows:

$$P(\theta) = \int \mathcal{E}(\theta_0)d\theta_0$$

$$+ \int \mathcal{E}(\theta_0)\cos(2\pi B_\lambda(\theta-\theta_0))d\theta_0 \quad (13)$$

$$\equiv S_0[1 + V(\theta, B_\lambda)], \quad (14)$$

where

$$S_0 \equiv \int \mathcal{E}(\theta_0)d\theta_0 \quad (15)$$

and

$$V(\theta, B_\lambda) \equiv \frac{1}{S_0}\int \mathcal{E}(\theta_0)\cos[2\pi B_\lambda(\theta-\theta_0)]d\theta_0 \quad (16)$$
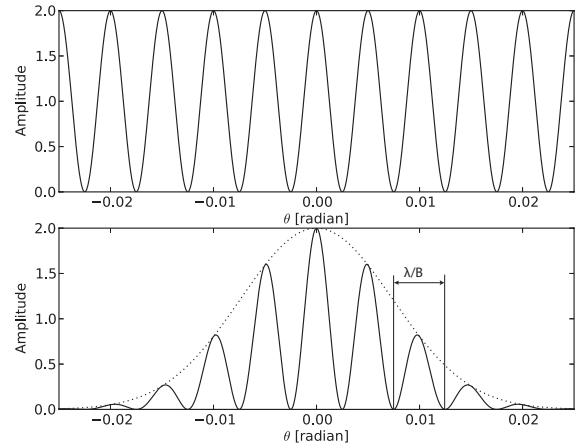

FIG. 3.— Example plots of the total power as a function of telescope pointing θ in the case of a point source. *Top:* Fringe pattern (eq. 12). *Bottom:* Fringe pattern attenuated by the telescope beam pattern. The dotted-line is a Gaussian beam pattern with a FWHM of 1 degree.

$$= \frac{1}{S_0}\left[\cos(2\pi B_\lambda\theta)\int \mathcal{E}(\theta_0)\cos(2\pi B_\lambda\theta_0)d\theta_0\right.$$

$$\left. + \sin(2\pi B_\lambda\theta)\int \mathcal{E}(\theta_0)\sin(2\pi B_\lambda\theta_0)d\theta_0\right] (17)$$

$$\equiv V_0(B_\lambda)\cos[2\pi B_\lambda(\theta - \Delta\theta)]. \quad (18)$$

Here, the visibility $V_0(B_\lambda)$ and the phase shift $\Delta\theta$ are defined as

$$V_0(B_\lambda)\cos(2\pi B_\lambda\Delta\theta) = \frac{1}{S_0}\int \mathcal{E}(\theta_0)\cos(2\pi B_\lambda\theta_0)d\theta_0 (19)$$

$$V_0(B_\lambda)\sin(2\pi B_\lambda\Delta\theta) = \frac{1}{S_0}\int \mathcal{E}(\theta_0)\sin(2\pi B_\lambda\theta_0)d\theta_0 (20)$$

which lead to

$$V_0(B_\lambda) = e^{i2\pi B_\lambda\Delta\theta}\frac{1}{S_0}\int \mathcal{E}(\theta_0)e^{-i2\pi B_\lambda\theta_0}d\theta_0. \quad (21)$$

The first term $e^{i2\pi B_\lambda\Delta\theta}$ is a phase shift $\Delta\theta$ of a complex visibility. The visibility amplitude is therefore

$$|V_0(B_\lambda)| = \left|\frac{1}{S_0}\int \mathcal{E}(\theta_0)e^{-i2\pi B_\lambda\theta_0}d\theta_0\right|. \quad (22)$$
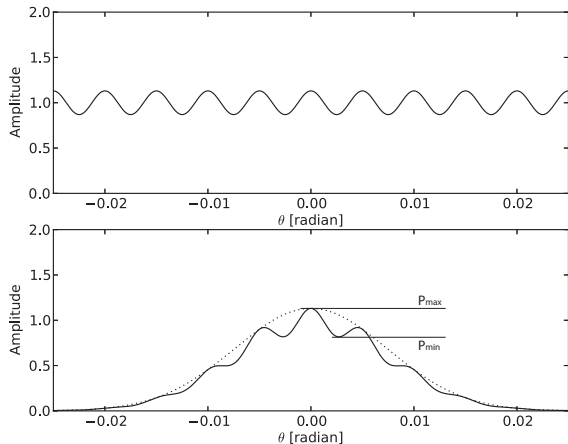
Fig. 4.— Example plots of the total power as a function of telescope pointing θ in case of disk (like the Sun). *Top:* Fringe pattern (eq. 12). *Bottom:* Fringe pattern attenuated by the telescope beam pattern. The dotted-line is a Gaussian beam pattern with a FWHM of 1 degree.

This is a Fourier component of the object $\mathcal{E}(\theta_0)$ at a baseline length of B_λ. The inverse $1/B_\lambda$ is the angular size of the Fourier component in radians. Observations at long baseline lengths detect structures of small angular size (i.e., Fourier components corresponding to small angular structures), while those at short baselines capture structures of large angular size.

Figure 4 (*top*) shows the theoretical fringe pattern for the top-hat function (e.g., the Sun's disk in 2-dimensions). The pattern is also attenuated by the beam pattern (Figure 4 *bottom*).

2.5. *Visibility Measurements and Sun's Diameter*

We measure $P(\theta)$ and calculate the visibility amplitude $|V_0(B_\lambda)|$. From eqs. (14) and (18), we have

$$P(\theta) = S_0\left[1 + V_0(B_\lambda)\cos\left[2\pi B_\lambda(\theta - \Delta\theta)\right]\right] \quad (23)$$

Figure 4 (*bottom*) is what we see toward the Sun – we sweep across the Sun by slewing the telescope in the azimuthal direction (i.e., changing θ). The fringe pattern is attenuated by the antenna response pattern, but we assume that the antenna response is approximately constant around the peak of the response pattern. The maximum and minimum powers of the sinusoidal curve (see Figure 4 *bottom*) are

$$P_{\max} = S_0[1 + V_0(B_\lambda)] \quad (24)$$
$$P_{\min} = S_0[1 - V_0(B_\lambda)]. \quad (25)$$

From these, we calculate

$$|V_0(B_\lambda)| = \frac{P_{\max} - P_{\min}}{P_{\max} + P_{\min}}. \quad (26)$$

This is the visibility amplitude at a baseline length of B_λ.

The two side mirrors slide on the ladder in Figure 1 and change the baseline length. We repeat measurements of $|V_0(B_\lambda)|$ at different baseline lengths and make a plot of $|V_0(B_\lambda)|$ as a function of B_λ. $|V_0(B_\lambda)|$ is a Fourier component of $\mathcal{E}(\theta_0)$; therefore, we should see the Fourier transformation of the emission distribution in the plot.
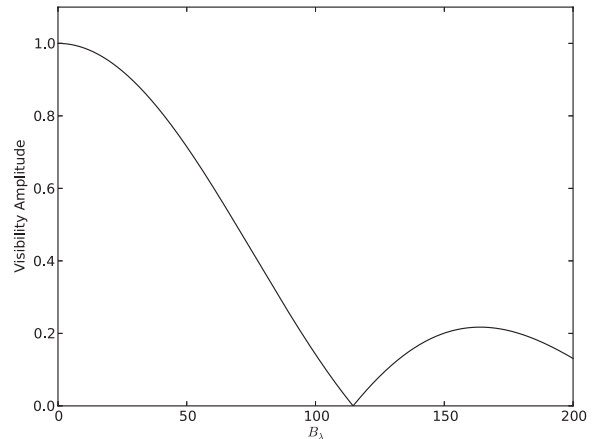

Fig. 5.— Visibility amplitude as a function of baseline length in the case of a disk.

The Sun's $\mathcal{E}(\theta_0)$ can be approximated as a top-hat function. Assuming the Sun's diameter is α, it is

$$\mathcal{E}(\theta_0) = \begin{cases} 1, & \text{if } |\theta_0| < \alpha/2 \\ 0, & \text{otherwise} \end{cases} \quad (27)$$

The Fourier transform is

$$|V_0(B_\lambda)| = \frac{\sin(\pi B_\lambda \alpha)}{\pi B_\lambda}. \quad (28)$$

This is a *sinc* function (Figure 5). By fitting, we determine the parameters of this *sinc* function, which can be translated to the diameter of the Sun α. (This is a 1-dimensional approximation of the Sun's shape. A more ambitious exercise would be to use a more accurate treatment of its 2-dimensional shape.)

3. INSTRUMENTS

We describe the construction of the telescope and receiver system. The budget is often the main limitation in the development of student lab experiments. Hence, we utilized low-cost parts and materials and used a commercial broadcast satellite dish and feedhorn operating at radio X-band. The system was constructed in our machine and electronics shops. Fabrication of the components could be offered as a student lab projects.

3.1. *Telescope and Optics*

Figure 1 shows the design of the Michelson stellar radio interferometer. Radio signals from the Sun hit two flat mirrors at the sides and are reflected to a satellite dish antenna by the central flat mirrors. The signals from the two sides are mixed as detected. Figure 6 shows photos of the telescope. It was built with mostly commercial products and materials. A broadcast satellite dish and feedhorn (blue in Figure 1; Figure 6a,b) operates at a frequency of $\nu \sim 11$ GHz ($\lambda \sim 2.7$ cm in wavelength). The required accuracy of optics at this wavelength is about $\sim$3-5 mm, which is relatively easy to achieve with flat mirrors (without curvature).

The flat mirrors (green in Figure 1) are made of fiberboard with wooden framing structures (Figure 6e). The mirror surfaces are all angled 45 deg from the optical path. We originally covered their surfaces with kitchen

aluminum foil, which has an appropriate thickness with respect to the skin depth ($\sim 0.8\mu m$) at the operating wavelength (reflectivity $\sim 96\%$ from our lab measurements). Later, we replaced it with thin aluminum plates as student-proofing (Figure 6d). The two side mirrors slide on a ladder to change the baseline length.

The azimuth-elevation mount structure is made with plywood (red in Figure 1 and blue and yellow in Figure 6). The azimuthal and elevation axes are driven with motors (Figure 6c), which are controlled by a paddle (i.e., handset in Figure 6b). The protractor (Figure 6f) is placed at the center of the bottom mount plate (yellow in Figure 6b) for measurement of the azimuthal angle of the telescope. Figure 6a shows the whole structure of the telescope. A metal pole is mounted perpendicular to the top mount plate (Figure 6b) and aluminum frame (Figure 6c), and supports the dish. Note that the pole should be perpendicular, which makes the pointing adjustment easier as discussed later.

The azimuthal rotation is facilitated by greased handcrafted ball bearings in circular grooves around the azimuth shaft on the base (blue in Figure 6a,b - below the yellow structure) and on the bottom mount plate (yellow).

Sweeping across the Sun in azimuth permits fringe measurements. This telescope can be converted to a single-dish telescope by flipping the satellite dish by 180 degrees around the metal pole (see Figure 6b). Single-dish and interferometer measurements can be easily made and compared, which is essential for appreciation of the high angular resolution possible with the interferometer.

Table 1 lists the commercial product parts that we purchased. The other parts, mostly the support structure, are made in the machine shop.

3.2. *Receiver System*

The signal detection system in radio astronomy is a series of electronic components. Figure 7 shows the design and photos of the receiver. Again, these are mostly commercial products.

Signals from the sky are at too high a frequency (~ 11 GHz) to be handled electronically. Hence the Low Noise Block Feedhorn (LNBF) down-converts the frequency to a lower frequency, called the intermediate frequency (IF; 950-1950MHz), by mixing the sky signal with a reference signal at a slightly-offset frequency and producing a signal at the beat frequency of the sky and reference signals. This is called heterodyne receiving. The LNBF works as a heterodyne mixer.

Figure 7 shows the flow of signal. In sequence, an amplifier, two attenuators, and bandpass filter adjust the signal amplitude to the input range of a square-law detector. We combined two commercially available attenuators to achieve the desired attenuation of ~ 16 db. A filter with a 100 MHz width narrows the frequency range, since the bandwidth of the IF (1GHz at the operating frequency of $\sim$11 GHz) is too broad for detection of null fringes in interferometry. Output from the detector is then amplified to the whole dynamic range of the analog-to-digital (A/D) converter. We assembled all these components inside a metal box for protection. A power supply is also in the box, providing the power to the LNBF and amplifiers.

The output from the receiver box goes to a commercial LabPro A/D convertor. The LabPro is connected via USB to, and controlled by, a laptop computer with LabPro software installed. It takes care of time integration and sampling rate for voltage measurements.

Table 2 lists the electronics components that we purchased. The square-law detector (Schottky diode detector) was purchased through eBay, and similar devices seem almost always on sale there. We then found and purchased the amplifier and attenuators to adjust the signal voltage amplitude to adjust the input range of the detector and the output range of the LNBF when the telescope is pointing toward the Sun and satellites.

4. SETUP AND MEASUREMENTS
4.1. *Setup*

The mount structure, ladder, and mirrors of the telescope (Figure 6) are detached when it is stored in our physics building. We move them with a cart to the front of the building and assemble them there on the morning of experiment. We make sure that the flat mirrors are angled at 45 deg with respect to the optical path and 90 deg vertically, using a triangle. We then attach the ladder and mirrors to the mount structure using clamps mounted on the structure.

The electronic components are also connected: the signal from the feedhorn goes to the receiver (Figure 7), then to the A/D converter LabPro, and finally to a computer via USB. We use software which comes with LabPro to control sampling frequency (integration time) and duration of recording.

Telescope pointing adjustment is the next step before the experiment. We prepare a table of the Sun's azimuthal and elevation angles as a function of time (e.g., at 10min interval) using an online tool provided by the U.S. Naval Observatory (http://aa.usno.navy.mil/data/docs/AltAz.php). The antenna is set to the single-dish mode (i.e., dish facing toward the Sun). We align the planes of the mount's top plate and ladder parallel to sunlight using their shadows. The azimuth is set to that of the Sun, and we adjust the elevation angle of the dish to maximize the signal from the Sun on the voltage meter. [Our dish is an off-axis paraboloid antenna, and the direction of the dish looks very offset from the direction of the Sun. We therefore need to use the voltage meter. We later installed a footlong rod on the dish and marked a point (on the dish) at which the shadow of the rod tip falls when pointed toward the Sun.] We then flip the dish by 180 deg around the metal pole for interferometer measurements.

The signal amplitudes from the two side mirrors need to be balanced. We check the voltage readout from each side mirror separately by blocking the optical path of the other (or by removing the other mirror). We move the central mirror toward the side of stronger signal to decrease its effective surface area.

4.2. *Measurements*

Once the mirrors are set and the telescope is pointed toward the Sun, we start interferometer measurements. We should see fringes from the Sun (e.g., Figure 4) as we slew the telescope and sweep across the Sun in the azimuthal direction. We typically spend 10-30 second on
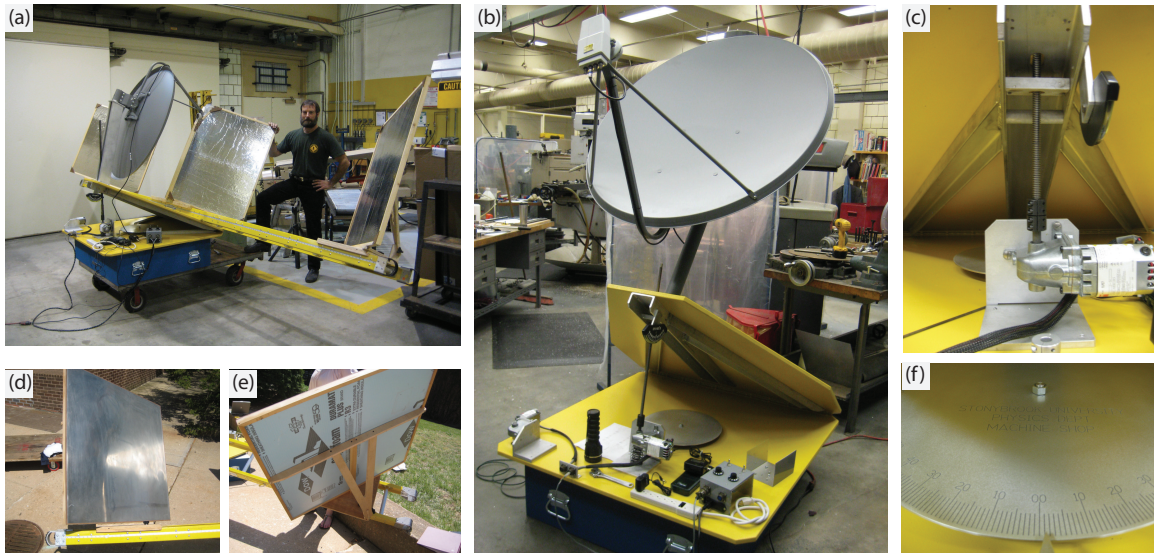
FIG. 6.— Photographs of the telescope. (a) Overall view. (b) Mount structure. The blue box at the bottom (with handles) and yellow plates are made of wood. The entire yellow part rotates in the azimuthal direction on the blue box. The two yellow plates are attached with hinges, and the top plate moves up to change the elevation angle. The telescope is shown in a "single-dish" mode, and the dish would be rotated by 180 deg for an "interferometer" experiment. (c) Support structure. The aluminum frame supports the telescope. A screw rod and elevation drive motor are also visibile. (d) Side mirror from the front side. Kitchen aluminum foil is thicker than the required skin depth, but we glued a thin aluminum plate instead, as student-proofing. (e) Side mirror from the backside. It's supported by a wood frame. (f) Protoractor to measure the azimuthal angle of the telescope.

each "sweep" observation, and then correct the telescope pointing before the next sweep. The pattern may be seen as variations of the voltage readout, or as a fringe pattern in a plot (Figure 4), if the LabPro and computer are already started. The LabPro and the computer do not know about telescope pointing and record only the readout voltage as a function of time. We therefore need to convert the time to azimuthal angle after the measurements. We record the start and end azimuthal angles in sweeping the Sun – we start from a far-off position, say 10-20deg away in azimuth, and sweep the Sun in azimuth. We assume that the telescope slew speed is constant (approximately correct when we record for a long time, e.g. 20-30 seconds). The projection effect, i.e., the cos(elevation) term, must be accounted for in calculation of arc length in the sky.

We change baseline length by sliding the side mirrors on the ladder and repeat fringe measurements. The baseline length should be determined from the fringe pattern, but for reference, we record the side mirror separation using a tape measure fixed to the ladder.

4.3. *Miscellaneous*

Radio interference was initially a problem. We conducted a site search across the campus. We brought the dish and a commercial receiver (called a satellite finder ~ $10-20, which is used to find commercial television satellites when a dish is installed) and compared the strengths of the Sun and ambient radio signals. We conveniently found that one spot in front of our building was radio quiet.

Geosynchronous satellites are located along a thin belt in the sky. The Sun's sidereal path gets aligned along this belt in some seasons, which hinders the experiment. This should be checked at the planning stage of the experiment.

The current mount structure is slightly wider than a standard doorway. It does not fit on most of our elevators and cannot pass through exit doors of our building. We have to carry it out via a loading deck. This could have been taken into account when the telescope was designed.

The telescope can be used as a single-dish radio telescope by pointing the dish directly toward the sky. The beam size of our dish is roughly $\sim 1\,$deg in X band, with which we can barely resolve the Sun ($\sim 1/2\,$deg diameter). We can compare the profiles of the Sun and a commercial satellite (a point source) to find this experimentally. The Sun's diameter can be resolved and determined with the interferometer. The comparison of the single-dish and interferometer measurements permits students to appreciate the superiority of interferometry in terms of spatial resolution.

5. RESULTS FROM A LAB REPORT

Figure 8 shows results from a student group's lab report, Panel (a) is an example of a fringe pattern of the Sun. They determined the baseline length by measuring the interval between peaks and troughs (and from their readings of the side mirror separation). This group repeated fringe measurements three times at each of 10 different baseline lengths. Panel (b) shows a fit of the *sinc* function, i.e., the Fourier transform of the Sun. The null point at $B_\lambda = 96$ in the fit suggests that their measurement of the sun's diameter is $\sim 36'$ at ~ 11 GHz. Note that its reported diameter at ~ 10 GHz is about $34'$ with little dependence on solar activity (i.e., sunspot number); this diameter is calculated from the observed radio-to-optical diameter ratios (Das, Sarkar, & Sen 2000) and the optical diameter of $\sim 30'$. These results demonstrate a proof of concept demonstrated by our students, and a variety of exercises can be developed for a student lab beyond what is described here.
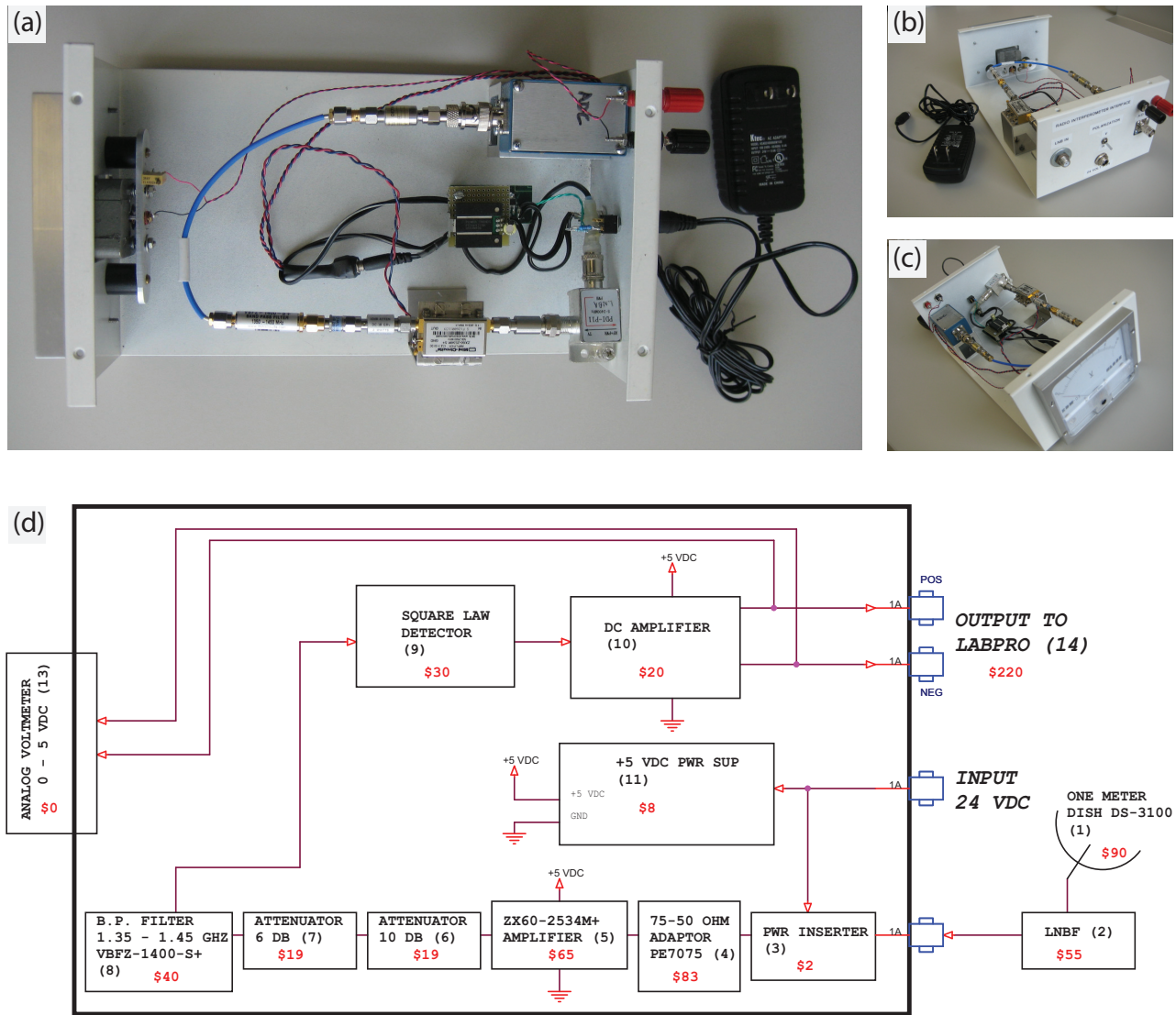
FIG. 7.— Photographs and schematic of the receiver. (a) Interior of receiver box. Most components are commercial. (b) Front side of the receiver box. Two critical plugs are for an input from the feedhorn and output to the LabPro (commercial analog/digital converter often used in physics lab courses, which outputs to a computer through a USB connection). (c) Back side. We installed an analog voltage meter, so that signal detection can be easily checked during observations. (d) Schematic diagram of receiver components.

REFERENCES

Michelson, A. A., & Pease, F. G., "Measurement of the diameter of alpha Orionis with the interferometer," 1921, ApJ, 53, 249-259

Michelson, A. A., & Morley, E. W., "On the Relative Motion of the Earth and of the Luminiferous Ether," 1887, Sidereal Messenger, vol. 6, pp.306-310, 6, 306

Melissinos, A. C. & Napolitano, J. 2003, "Experiments in Modern Physics", Academic Press.

Serway, R. A. & Jewett, J. W. 2013, "Physics for Scientists and Engineers", Cengage Learning

Bennett, J. O., Donahue, M., Schneider, N. & Voit, M. 2013, "The Cosmic Perspective", Addison-Wesley

Wolfson, R., & Pasachoff, J. M. 1999, "Physics for Scientists and Engineers", Addison Wesley

Fang, Guangyu, Huang, Li, Xin, Li, Zhao, Haifa, Huo, Lei, & Wu, Lili, "Geometric explanation of conic-section interference fringes in a Michelson interferometer," 2013, American Journal of Physics 81, 670-675

Rudmin, J. W., Taylor, G. R., Hand, P. M., Ashworth, J. N., & Wehr, P. H., "Simple ultra-low-cost undergraduate holography using a modified Michelson interferometer," 1980, American Journal of Physics 48, 746-748

Matthys, D. R. & Pedrotti, F. L., "Fourier transforms and the use of a microcomputer in the advanced undergraduate laboratory," 1982, American Journal of Physics 50, 990-995

Da Costa, German, Kiedansky, Gerardo, & Siri, Ricardo, "Optoelectronic seismograph using a Michelson interferometer with a sliding mirror," 1988, American Journal of Physics 56, 993-997

TABLE 1
COMMERCIAL PRODUCTS PURCHASED FOR TELESCOPE MOUNT

No	Description	Quantity	Manufacturer	Part No.	Vendor	Price
1	Manhole Ladder 16 ft	1	Werner	M7116-1	Lowe's	$226
2	Motor	2	Dayton	1LPZ7	Walmart	$248
3	Lev-O-Gage	1	Sun Company, Inc.	NWH-0152-1003	opentip.com	$18

TABLE 2
PURCHASED RECEIVER PARTS

No	Description	Quantity	Manufacturer	Part No.	Vendor	Price
1	1-Meter Satellite Dish	1	WINEGARD	DS-3100	Solid Signal	$90
2	Quad Polar LNBF	1	INVACOM	QPH-031	SatPro.tv	$55
3	Power Inserter	1	PDI	PDI-PI-1	Solid Signal	$2
4	75-50 Ohm Adaptor	1	PASTERNACK	PE7075	Pasternack	$83
5	Amplifier 501/2 0.5 to 2.5 GHz	1	Mini-Circuits	ZX60-2534M+	Mini-Circuits	$65
6	Attenuator SMA 3GHz 50 Ohm 10db	1	Crystek	CATTEN-0100	Digi-Key	$19
7	Attenuator SMA 3GHz 50 Ohm 6db	1	Crystek	CATTEN-06R0	Digi-Key	$19
8	Bandpass Filter 1350 to 1450 MHz	1	Mini-Circuits	ZX60-2534M+	Mini-Circuits	$40
9	Square-Law Detector 1.0-15.0 GHz	1	Omni Spectra	Model 20760	eBay	$30
10	5X OP-Amp	1	Custom Built[a]			$20
11	IC Buck Converter Mod 5.0V SIP3	1	ROHM	BP5277-50	Digi-Key	$8
12	Box Aluminum 4'×6'×10' (HWD)	1	LMB Heeger	UNC 4-6-10	DigiKey	$45
13	0-5V Analog Meter 4¨	1	Salvaged			$0
14	Data Converter & Collection	1	Vernier	LabPro	Vernier	$220

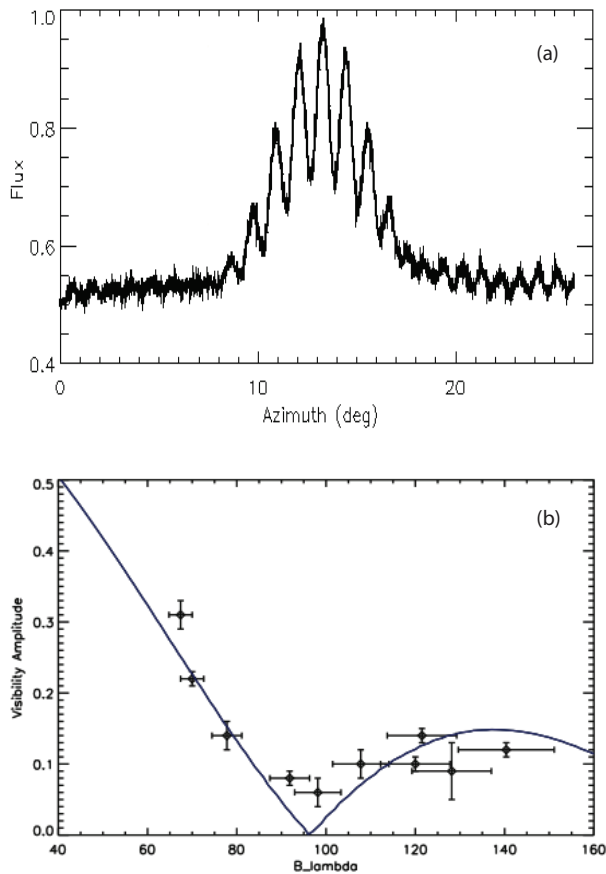[a]This component could be simply some batteries that provide the voltage of ~ 5 V.

Fig. 8.— Results from a student report. (a) Measured fringes from the Sun. (b) Visibility amplitude vs baseline length [in λ].

Diamond, Joshua B., Donnelly, Denis P., Breault, James D., & McCarthy, Mary E., "Measuring small vibrations with interferometry," 1990, American Journal of Physics 58, 919-922

Mellen, Walter Roy, "Interference patterns from circularly polarized light using a Michelson interferometer," 1990, American Journal of Physics 58, 580-581

Norman, Jeffrey B., "Phase-conjugate Michelson interferometers for all?optical image processing and computing," 1992, American Journal of Physics 60, 212-220

Belansky, Richard H. & Wanser, Keith H., "Laser Doppler velocimetry using a bulk optic Michelson interferometer: A student laboratory experiment," 1993, American Journal of Physics 61, 1014-1019

Kiess, Thomas E. & Berg, Richard E., "Dominant color reversals and chromaticity cusps in interferometric color mixing," 1996, American Journal of Physics 64, 928-934

Nachman, Paul , Pellegrino, Paul M., & Bernstein, Aaron C., "Mechanical resonance detected with a Michelson interferometer," 1997, American Journal of Physics 65, 441-443

Fox, P. J., Scholten, R. E., Walkiewicz, M. R., & Drullinger, R. E., "A reliable, compact, and low-cost Michelson wavemeter for laser wavelength measurement," 1999, American Journal of Physics 67, 624-630

Kuroda, K., Ohashi, M., Miyoki, S., et al., "Large-Scale Cryogenic Gravitational Wave Telescope," 1999, International Journal of Modern Physics D, 8, 557-579

Abbott, B. P., Abbott, R., Adhikari, R., et al., "LIGO: the Laser Interferometer Gravitational-Wave Observatory," 2009, Reports on Progress in Physics, 72, 076901

Harry, G. M., & LIGO Scientific Collaboration, "Advanced LIGO: the next generation of gravitational wave detectors ," 2010, Classical and Quantum Gravity, 27, 084006

Pawsey, J. L., Bracewell, R. N. 1955, "Radio Astronomy", Oxford University Press

Steinberg, J. L., & Lequeux, J. 1963, "Radio Astronomy", McGraw-Hill Book Company, Inc.

Christiansen, W. N., & Högbom, J. A. 1985, "Radiotelescopes", Cambridge University Press

Wilson, T. L., Rohlfs, K., & Hüttemeister, S. 2013, "Tools of Radio Astronomy", Springer

Taylor, G. B. and Garilli, C. L. and Perley, R. A. 1999, "Synthesis Imaging in Radio Astronomy II", ASP Conference Series, 181.

Thompson, A. R., Moran, J. M., and Swenson, G. W. 2007, "Interferometry and Synthesis in Radio Astronomy", John Wiley & Sons.

Pryor, Marvin J., "Measuring Artificial Star Separation by Interference," 1959, American Journal of Physics 27, 101-103

Illarramendi, M. A., Hueso, R., Zubia, J., Aldabaldetreku, G., Durana, G., & Sánchez-Lavega, A., "A daylight experiment for teaching stellar interferometry," 2014, American Journal of Physics 82, 649-653

Shao, M., & Colavita, M. M., "Long-baseline optical and infrared stellar interferometry," 1992, ARA&A, 30, 457-498

Quirrenbach, A., "Optical Interferometry," 2001, ARA&A, 39, 353-401

Monnier, J. D., "Optical interferometry in astronomy," 2003, Reports on Progress in Physics, 66, 789-857

Das, T. K., Sarkar, H. and Sen A. K., "The ratio of the radio and optical diameters of the sun at centimeter wavelengths," 2000, Solar Physics, 194, 155-163